Mathematical Geosciences
https://doi.org/10.1007/s11004-024-10135-8

Scale-Independent Variation Rates of Phanerozoic Environmental Variables and Implications for Earth's Sustainability and Habitability

Haitao Shang[1]

Received: 20 April 2023 / Accepted: 15 January 2024

Abstract
The atmospheric CO_2 level, global average temperature, and sea level, which are three key metrics characterizing Earth's surface environments, underwent a series of significant changes over geologic time. Here, I investigate the variation rates of these three variables during the Phanerozoic Eon and show that they systematically exhibit scale-independent behaviors. I then derive a general mathematical form of these scale-independent patterns based on geosystem-specific assumptions and basic physical principles. From the perspective of statistical mechanics, these scale-independent behaviors appearing in the planetary-scale geological system imply that the internal dynamics and interactions of different components in the Earth system have significantly influenced its evolution and stability, which sheds light on Earth's sustainability and habitability.

Keywords Scale independence · Variation rates · Environmental variables · Atmospheric CO_2 level · Global average temperature · Sea level · Phanerozoic Eon · Sustainability and habitability

1 Introduction

The Phanerozoic Eon, which spans from around 540 million years ago (Ma) to the present, witnessed a series of spatial and temporal variations in the geological system. Modern geochemical techniques and theoretical models are remarkably successful at reconstructing the history of environmental variables characterizing the geological system, such as the atmospheric CO_2 level, global average temperature, and sea level. These variables serve as proxies for the evolutionary trajectories of the Earth's surface environment and are closely tied to the course of life evolution. The CO_2 fluxes

✉ Haitao Shang
htshang.research@gmail.com

[1] Institute of Ecology and Evolution, University of Oregon, Eugene, OR 97403, USA

Published online: 21 March 2024

throughout the atmosphere, lithosphere, and biosphere; variations in CO_2 levels reflect the changes in geological and biological aspects of Earth's carbon cycle (Hayes and Waldbauer 2006; Royer et al. 2001). Temperature significantly influences the redox states of seawater (Huang and Schmitt 2014; Song et al. 2019) and the metabolisms and evolution of marine life (Mayhew et al. 2012; Song et al. 2021). Fluctuations of the sea level account for the radiation, diversity, and extinction of life on the ancient Earth (Hallam and Wignall 1999; Kocsis and Scotese 2021), potentially via species-area effects (Peters 2007); the patterns of sea-level variations recorded in sedimentary rocks have been shown to be consistent with the Phanerozoic macroevolutionary trends of marine animals (Peters 2005; Hannisdal and Peters 2011).

Scale independence is a key feature of the power-law pattern, a functional relation between two variables in which one varies as a power of the other. Generally, power laws are expressed as $y(x) \propto x^{-\phi}$, where x and y are two variables and $\phi > 0$ is a scaling parameter. On a log–log plot, they appear as a straight line, $\log_{10}(y) \propto -\phi \log_{10}(x)$, indicating that the underlying regularity of such a pattern does not depend on specific scales (Bak 2013; Schroeder 2009). Scale-independent patterns exist widely in various natural systems (Bak 2013; Schroeder 2009); for instance, the degradation rate constant versus age of organic matter in aquatic systems (Middelburg 1989; Shang 2023b) and the frequency versus magnitude of earthquakes (Cannavò and Nunnari 2016; Bak et al. 2002) have been shown to exhibit scale-independent behaviors. However, such behaviors on the ancient Earth have rarely been explored; the best known one is the power law of the frequency versus size of extinction events in the Phanerozoic biological system (Raup 1986; Bak 2013). Whether such patterns existed in the deep-time geological system remains unknown. Here, I investigate three representative environmental variables characterizing the Phanerozoic geological system—atmospheric CO_2 level, global average temperature, and sea level—and demonstrate that the variation rates in these variables exhibited scale-independent patterns.

This work is structured as follows. Section 2 describes the processes of data processing, power-law fitting, goodness-of-fit test, and likelihood-ratio tests. Section 3.1 shows the scale-independent behaviors in the variation rates of atmospheric CO_2 level, global average temperature, and sea level on log–log plots (Fig. 1) and presents the mathematical expressions and statistical analyses of the best-fitting power laws (Table 1). In Sect. 3.2, I derive a general form of these scale-independent behaviors with some basic physical principles and geosystem-specific assumptions, which offers an interpretation for the origin of these patterns from the perspective of thermodynamics. Section 3.3 discusses the implications of these scale-independent patterns for the stability and internal dynamics of the deep-time geological system and the sustainability and habitability of the modern Earth. This work shows for the first time that power-law behaviors appear in the Phanerozoic environmental variables and suggests that such patterns manifest the intrinsic dynamics of a planetary-scale system over geologic time.

2 Materials and Methods

2.1 Data

The datasets on the Phanerozoic atmospheric CO_2 level, global average temperature, and sea level are obtained from studies by Foster et al. (2017), Scotese et al. (2021), and Boulila et al. (2018), respectively. To better analyze the scale-independent patterns, which usually span several orders of magnitude, I interpolate each dataset with smoothing splines (De Boor 1978), which have been shown to be effective for fitting the time series for each of these environmental variables (Vérard and Veizer 2019; Foster and Rohling 2013; Berner 1990) at geologic timescales. I then calculate the data value at every 0.1 million years with the best-fitting spline for each dataset. I denote a time series in a given dataset as $\{m_i\}$, where m_i is the mean of data points at time point i. For each dataset, I take the difference between the data values at every two consecutive time points (i.e., m_i and m_{i+1}) and express the variation rate at time point i as $R_i = (m_{i+1} - m_i)/\Delta t$, where Δt is the step size. The R_i values are classified into three categories: decrease (D), increase (I), and change (C). Logarithms of negative values are undefined; absolute values of variation rates in these three categories, which are denoted by $|R^{\mathrm{D}}| = \{|R_i| \big| R_i < 0\}$, $|R^{\mathrm{I}}| = \{R_i \big| R_i > 0\}$, and $|R^{\mathrm{C}}| = \{|R_i| \big| R_i \neq 0\}$, are used to investigate the scale-independent patterns in these datasets. Obviously, $|R^{\mathrm{C}}|$ is the union of $|R^{\mathrm{D}}|$ and $|R^{\mathrm{I}}|$: $|R^{\mathrm{C}}| = |R^{\mathrm{D}}| \cup |R^{\mathrm{I}}|$. Zero values of R_i are not considered in the analyses not only because the logarithm of zero is undefined but also because a zero value indicates no variation.

2.2 Power-Law Fitting

Based on Sturges' rule (Scott 2009), I determine the optimal number of bins (N_{bin}) for a dataset using $N_{\mathrm{bin}} = \log_2(N_{\mathrm{data}}) + 1$, where N_{data} is the specific number of data points in this dataset. I denote the number of data points in each category of $|R^{\mathrm{D}}|$, $|R^{\mathrm{I}}|$, and $|R^{\mathrm{C}}|$ by $N_{\mathrm{data,D}}$, $N_{\mathrm{data,I}}$, and $N_{\mathrm{data,C}}$, respectively. Correspondingly, the optimal numbers of bins for these three categories are $N_{\mathrm{data,D}} = \log_2(N_{\mathrm{data,D}}) + 1$, $N_{\mathrm{data,I}} = \log_2(N_{\mathrm{data,I}}) + 1$, and $N_{\mathrm{data,C}} = \log_2(N_{\mathrm{data,C}}) + 1$, respectively; the empty bins are discarded. For data in a category of one quantity, I denote the total number of bins by J and the number of data points in the jth bin by N_j; the set $\{N_0, N_1, \ldots, N_J\}$, which is a collection of the numbers of data points in each bin, is henceforth denoted by $\{N_j\}_{j=0}^{J}$.

A key property of power-law distributions is their right tails, where extreme values of random variables appear. Occasionally, small values on the left side of the distribution may not follow a power law; these data points with small values are not used in data fitting (Clauset et al. 2009; Alstott et al. 2014). To determine the place to truncate the set of counts $\{N_j\}_{j=0}^{J}$, one needs to identify the point where the power-law relation begins; I denote this truncation point as N_{min}. To determine N_{min}, I establish a power-law fit starting from each individual data point in $\{N_j\}_{j=0}^{J}$ and then select the point generating the minimum distance between the fit and the data (Clauset et al. 2009; Alstott et al. 2014). More specifically, I denote the subset of $\{N_j\}_{j=0}^{J}$ that starts from

the point N_l by $K_l = \{N_j\}_{j=l}^{J} = \{N_l, N_{l+1}, \ldots, N_J\}$, fit data points in each of these subsets (i.e., $K_0, K_1, \ldots, K_{J-1}$) on log–log plots, and calculate the error (denoted by ϵ_l) between the data and the fit for each subset (Clauset et al. 2009; Alstott et al. 2014); the minimum error for all subsets is denoted as $\epsilon_{\min} = \min\{\epsilon_l\}$. The subset K_l corresponding to $\epsilon_{\min}$ is the optimal subset for the power-law fitting and is denoted by $K_{l,\text{opt}}$. The initial point in the subset $K_{l,\text{opt}}$ then is the optimal truncation point $N_{\min}$ defined above. The power law that best fits the truncated dataset $K_{l,\text{opt}}$ starting at point $N_{\min}$ is the optimal power law.

2.3 Goodness-of-Fit Tests

To assess the goodness of fit of the power laws, I first compute the coefficients of determination (R^2) and root mean square errors (RMSEs). The R^2 measures the proportion of the variation in the dependent variable that can be explained by the best-fitting power laws. The value of R^2 generally ranges from 0 to 1; a larger value of R^2 indicates a better-fitting and therefore a more reliable model (Freund and Wilson 2003). The RMSE measures the distance between actual and predicted values; a small RMSE value suggests a good fit. The Kolmogorov–Smirnov (KS) test (Massey Jr 1951) and Cramér–von Mises (CM) two-sample test (Anderson 1962) are also used to evaluate the goodness of fit of the power laws. The KS statistic is defined as the maximum distance between the cumulative distribution functions (CDFs) of the power law that best fits the data (G_{M}) and the data themselves (G_{D}): $\max|G_{\text{M}} - G_{\text{D}}|$ (Massey Jr 1951). The CM statistic is defined as $\left(\sum_{i=0}^{I}[G_{\text{M}}(x_i) - G_{\text{D}}(x_i)]^2 + \sum_{j=0}^{J}\left[G_{\text{M}}(x'_j) - G_{\text{D}}(x'_j)\right]^2\right) \times \frac{I \times J}{(I+J)^2}$, where $\{x_i\}_{i=0}^{I}$ and $\{x'_j\}_{j=0}^{J}$ are data independently sampled from two distributions with G_{M} and G_{D} as the CDFs, respectively (Anderson 1962). I define the null hypothesis as $H_0 : G_{\text{M}} = G_{\text{D}}$ and the two-sided alternative as $H_1 : G_{\text{M}} \neq G_{\text{D}}$. The critical p value for these tests is set as 0.05. When p is less than or equal to 0.05, a power law does not fit the data well; when p is greater than 0.05, a power law adequately describes the data.

2.4 Likelihood-Ratio Tests

As a property of the power-law distribution, a straight line on a log–log plot is a necessary but not sufficient condition for the power-law pattern. Other heavy-tailed processes, such as the stretched exponential or lognormal distribution, may generate datasets with distributions that are close to power-law patterns due to sampling fluctuations. To determine which distribution better fits the data, I perform the likelihood-ratio test (Clauset et al. 2009): $\mathcal{R} = \log\left(\frac{\mathcal{L}_{\text{P}}(N_{\text{counts,opt}}|\widehat{\Theta_{\text{P}}})}{\mathcal{L}_{\text{A}}(N_{\text{counts,opt}}|\widehat{\Theta_{\text{A}}})}\right)$. In this formula of $\mathcal{R}$, $\mathcal{L}_{\text{P}}$ is the likelihood, fitted using the procedure described above, under the hypothesis of a power-law distribution; $\mathcal{L}_{\text{A}}$ is the likelihood, fitted with maximum likelihood estimation, under the hypothesis of an alternative distribution; and $\widehat{\Theta_{\text{P}}}$ and $\widehat{\Theta_{\text{A}}}$ are

the values of model parameters that maximize the likelihood functions $\mathcal{L}_{\mathrm{P}}$ and $\mathcal{L}_{\mathrm{A}}$, respectively, in the parameter space. If the value of $\mathcal{R}$ is positive, then the model under the hypothesis of a power-law distribution (i.e., the model corresponding to $\mathcal{L}_{\mathrm{P}}$) outperforms the model under the hypothesis of an alternative distribution (i.e., the model corresponding to $\mathcal{L}_{\mathrm{A}}$); if $\mathcal{R}$ is negative, then the model under the hypothesis of the alternative distribution prevails. Moreover, to correct for random fluctuations, I follow Vuong (1989) and Clauset et al. (2009), standardize $\mathcal{R}$ by the standard deviation, and obtain a p value to determine whether the sign (i.e., negative or positive value) of $\mathcal{R}$ is statistically significant. I set the significance level for the p value to 0.05. When p is less than 0.05, the test value of $\mathcal{R}$ is unlikely to derive from chance fluctuations; however, when p is greater than or equal to, the test value of $\mathcal{R}$ is inconclusive and the test fails to indicate that one distribution outperforms the other for the given dataset.

3 Results and Discussion

3.1 Scale-Independent Variation Rates

The variation rates of environmental variables are classified into three categories: negative ($|R^{\mathrm{D}}|$), positive ($|R^{\mathrm{I}}|$), and all ($|R^{\mathrm{C}}|$). The mathematical definitions of these three categories are provided in Sect. 2.1. Figure 1 illustrates power-law behaviors in the variation rates of (A–C) atmospheric CO_2 level (red circles), (D–F) global average temperature (blue circles), and (G–I) sea level (green circles). Table 1 summarizes the mathematical expressions of the optimal power laws (purple straight lines in Fig. 1) for these datasets (Sect. 2.2) and statistical metrics (i.e., R^2 values, RMSEs, and the p values of the KS and CM tests) measuring the goodness of fit of these power laws (Sect. 2.3). The results presented in Table 1 show that all fitted power laws have high R^2 values and low RMSEs; the p values of their KS and CM tests are all much greater than the critical threshold of 0.05 (Sect. 2.3). These results suggest that the mathematical formulas of the power laws in Table 1 fit the data well.

Although the results presented in Fig. 1 and Table 1 are plausible, further analyses are required to test the performance of the best-fitting power laws against other heavy-tailed distributions (e.g., stretched exponential and lognormal distributions), since the latter may result in datasets that have power law-like distributions because of chance fluctuations. To do so, I conduct the likelihood-ratio test (Sect. 2.4); the standardized likelihood ratios ($\mathcal{R}$) and their associated p values are presented in Table 2. For most of these likelihood-ratio tests, the $\mathcal{R}$ values are positive and the accompanying p values are less than the critical value 0.05, suggesting that the corresponding power laws outperform alternative distributions (Sect. 2.4). The only exceptions are the tests for the power law against the lognormal distribution for $|R^{\mathrm{D}}_{\mathrm{CO_2}}|$ and $|R^{\mathrm{I}}_{\mathrm{SL}}|$. In these two cases, although $\mathcal{R}_{\mathrm{LN}}$ values are positive, the associated p_{LN} values are greater than 0.05, indicating that these tests are inconclusive (Sect. 2.4) and that both power laws and lognormal distributions may provide plausible fits for $|R^{\mathrm{D}}_{\mathrm{CO_2}}|$ and $|R^{\mathrm{I}}_{\mathrm{SL}}|$. Nevertheless, the generally better performance of power laws over the alternative distributions for the variation rates of the three environmental variables (Table 2) and the systematic power-law patterns presented in Fig. 1 and Table 1 together suggest that

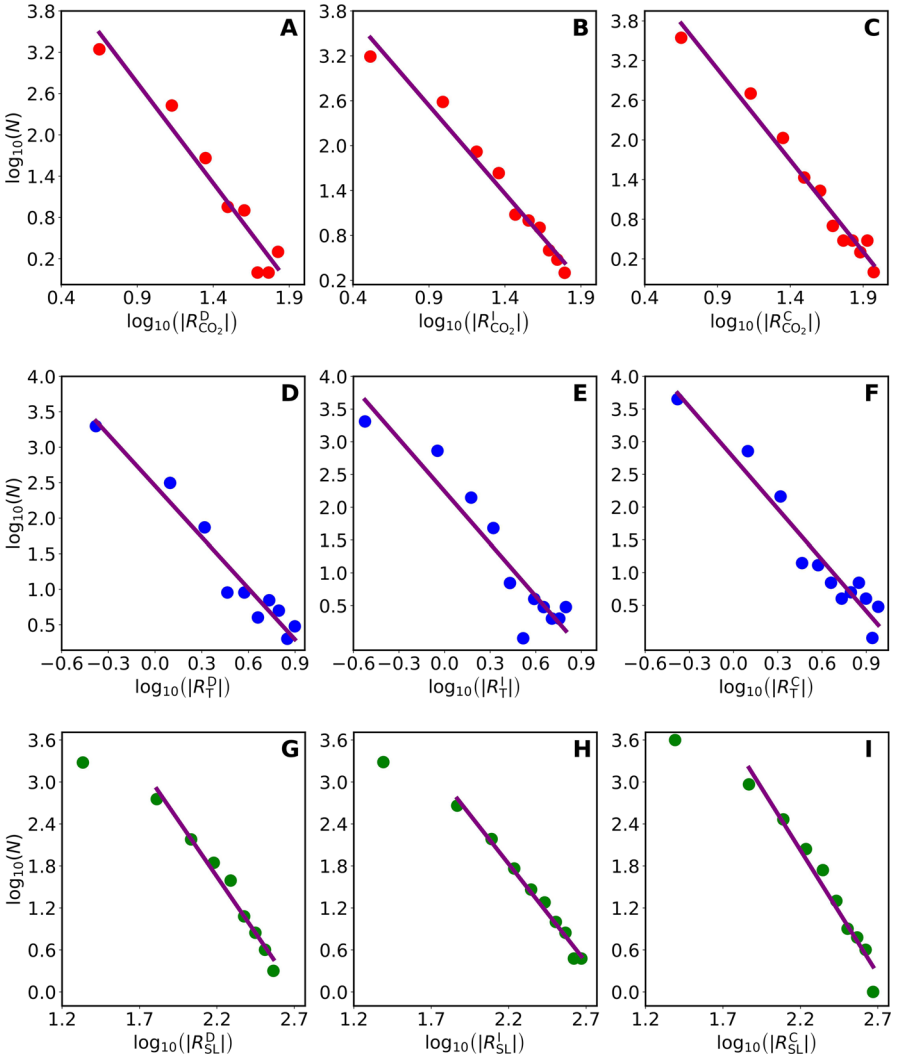

Fig. 1 Power laws of the negative ($|R^{\mathrm{D}}|$), positive ($|R^{\mathrm{I}}|$), and all ($|R^{\mathrm{C}}|$) variation rates of **A**–**C** atmospheric CO_2 level, **D**–**F** global average temperature, and **G**–**I** sea level in the Phanerozoic. Red, blue, and green circles represent the counts (i.e., N's) versus variation rates (i.e., $|R_i|$ values defined in Sect. 2.1) for atmospheric CO_2 level, global average temperature, and sea level, respectively. The initial small values in panels (**G**–**I**) that do not follow power laws are not included in data fitting (Sect. 2.2). Purple lines are the best-fitting power laws for the data. The mathematical expressions of power laws, the R^2 values and RMSEs of the best-fitting lines, and the KS and CM p values for goodness-of-fit tests (Sect. 2.3) are provided in Table 1. The likelihood-ratio tests for best-fitting power laws against alternative distributions (Sect. 2.4) are presented in Table 2

Table 1 Power laws of the negative ($|R^{\mathrm{D}}|$), positive ($|R^{\mathrm{I}}|$), and all ($|R^{\mathrm{C}}|$) variation rates of atmospheric CO_2 level, global average temperature, and sea level in the Phanerozoic

Quantity	Type of variation rate	Power law	R^2	RMSE	p_{KS}	p_{CM}
Variation rate of CO_2 level (R_{CO_2})	Negative	$N \sim (\lvert R^{\mathrm{D}}_{CO_2}\rvert)^{-2.91}$	0.95	0.15	0.99	0.87
	Positive	$N \sim (\lvert R^{\mathrm{I}}_{CO_2}\rvert)^{-2.35}$	0.94	0.11	1.00	0.98
	All	$N \sim (\lvert R^{\mathrm{C}}_{CO_2}\rvert)^{-2.76}$	0.93	0.16	1.00	1.00
Variation rate of temperature (R_{T})	Negative	$N \sim (\lvert R^{\mathrm{D}}_{\mathrm{T}}\rvert)^{-2.41}$	0.91	0.24	1.00	0.96
	Positive	$N \sim (\lvert R^{\mathrm{D}}_{\mathrm{T}}\rvert)^{-2.67}$	0.95	0.11	1.00	1.00
	All	$N \sim (\lvert R^{\mathrm{C}}_{\mathrm{T}}\rvert)^{-2.60}$	0.97	0.11	1.00	1.00
Variation rate of sea level (R_{SL})	Negative	$N \sim (\lvert R^{\mathrm{D}}_{\mathrm{SL}}\rvert)^{-3.23}$	0.88	0.24	0.98	0.98
	Positive	$N \sim (\lvert R^{\mathrm{I}}_{\mathrm{SL}}\rvert)^{-2.81}$	0.95	0.21	0.81	0.98
	All	$N \sim (\lvert R^{\mathrm{C}}_{\mathrm{SL}}\rvert)^{-3.54}$	0.91	0.28	0.98	0.98

The R^2, RMSE, p_{KS}, and p_{CM} represent the coefficient of determination, root mean square error, the p value of the KS test, and the p value of the CM test, respectively, of the best-fitting power laws. The value of R^2 ranges from 0 to 1. A large R^2 and a small RMSE imply a good fit. The critical p value for p_{KS} and p_{CM} is 0.05. A p_{KS} or p_{CM} greater than 0.05 suggests that a power law fits the data well; otherwise, a power law does not adequately describe the data

Table 2 Likelihood-ratio tests for the best-fitting power law against alternative distributions for each of the datasets on atmospheric CO_2 level, global average temperature, and sea level in the Phanerozoic

Quantity	Type	$\mathcal{R}_{\text{Exp}}$	p_{Exp}	$\mathcal{R}_{\text{S-Exp}}$	$p_{\text{S-Exp}}$	$\mathcal{R}_{\text{LN}}$	p_{LN}
Variation rate of CO_2 level (R_{CO_2})	Negative ($\lvert R^{\text{D}}_{CO_2}\rvert$)	2.21	0.008	1.05	0.042	0.96	0.135
	Positive ($\lvert R^{\text{I}}_{CO_2}\rvert$)	2.33	0.003	1.19	0.013	1.12	0.041
	All ($\lvert R^{\text{C}}_{CO_2}\rvert$)	1.41	0.007	0.82	0.025	0.44	0.033
Variation rate of temperature (R_{T})	Negative ($\lvert R^{\text{D}}_{\text{T}}\rvert$)	2.78	0.006	1.95	0.018	1.23	0.026
	Positive ($\lvert R^{\text{I}}_{\text{T}}\rvert$)	1.43	0.001	0.82	0.024	0.82	0.031
	All ($\lvert R^{\text{C}}_{\text{T}}\rvert$)	2.93	0.004	0.91	0.013	0.76	0.027
Variation rate of sea level (R_{SL})	Negative ($\lvert R^{\text{D}}_{\text{SL}}\rvert$)	2.33	0.002	1.43	0.022	1.27	0.035
	Positive ($\lvert R^{\text{I}}_{\text{SL}}\rvert$)	1.91	0.004	1.17	0.034	1.05	0.193
	All ($\lvert R^{\text{C}}_{\text{SL}}\rvert$)	2.26	0.008	1.24	0.018	1.35	0.037

The log-likelihood ratios (Sect. 2.4) for the best-fitting power law against exponential, stretched exponential, and lognormal distributions are denoted by $\mathcal{R}_{\text{Exp}}$, $\mathcal{R}_{\text{S-Exp}}$, and $\mathcal{R}_{\text{LN}}$, respectively. The p values for the statistical significance of these tests (Sect. 2.4) are p_{Exp}, $p_{\text{S-Exp}}$, and p_{LN}, respectively. A positive ratio indicates that the best-fitting power law outperforms the alternative for a given dataset, while a negative ratio suggests that the alternative prevails. When p is greater than or equal to 0.05, a likelihood-ratio test is inconclusive; however, when p is less than 0.05, a likelihood-ratio test is conclusive because it is unlikely to be influenced by random fluctuations

the power-law relation also serves as a better option for fitting $|R^{\mathrm{D}}_{\mathrm{CO_2}}|$ and $|R^{\mathrm{I}}_{\mathrm{SL}}|$ than the lognormal distribution.

3.2 A Model of Scale-Independent Patterns in the Geological System

The atmospheric CO_2 level, global average temperature, and sea level characterize various aspects of the Earth system; their variation rates thus should manifest the changes in the states of the geological system or some of its components. Here, I denote the realizations of an environmental variable at two consecutive time points, k and $k+1$, as m_k and m_{k+1}, respectively. I denote the entropies corresponding to states m_k and m_{k+1} by $E_k = -\log p(m_k)$ and $E_{k+1} = -\log p(m_{k+1})$, where $p(m_k)$ is the probability that the realization m_k occurs, and E_k characterizes the extent to which the system at the state corresponding to the realization m_k deviates from the equilibrium. I denote the difference between m_k and m_{k+1} by Δm_k and the variation in entropy when the realization of an environmental variable changes from m_k to m_{k+1} by ΔE_k. The variation rate at time point k is then expressed as

$$R_k = \frac{\Delta m_k}{\Delta t}, \tag{1}$$

where Δt is the time step between two consecutive time points k and $k+1$. For convenience, I assume in the following derivation that m_k is less than m_{k+1}, so that both Δm_k and R_k are positive for all t; therefore, both $\log(\Delta m_k)$ and $\log(R_k)$ are always mathematically well-defined. For the case when m_k is larger than m_{k+1}, one can arrive at the same general form of the scale-independent patterns presented below via replacing Δm_k and R_t in the following derivation by the absolute values $|\Delta m_k|$ and $|R_k|$, respectively (refer to the definitions of $|R^{\mathrm{D}}|$, $|R^{\mathrm{I}}|$, and $|R^{\mathrm{C}}|$ in Sect. 2.1). In this work, I do not consider the case when m_k and m_{k+1} are equal because $\log(\Delta m_k)$ and $\log(R_k)$ are mathematically undefined when $\Delta m_k = R_k = 0$.

From Eq. (1), I obtain $\Delta E_k = -\log p(\Delta m_k) = -\log p(R_k \cdot \Delta t)$ based on the additivity of entropy (Skilling 1989; Almeida 2003). Since the Δt is constant, I get $p(R_k \cdot \Delta t) = p(R_k) \cdot \Delta t \sim p(R_k)$ and $\log p(R_k \cdot \Delta t) = \log p(R_k) + \log(\Delta t) \sim \log p(R_k)$. In a continuous form, the expectation of ΔE_k can be expressed as

$$\langle \Delta E_k \rangle = -\int p(\Delta m_k) \cdot \log p(\Delta m_k)\, \mathrm{d}\Delta m_k \sim -\int p(R_k) \cdot \log p(R_k)\, \mathrm{d}R_k, \tag{2}$$

where $\langle \cdot \rangle$ represents the average of a quantity, and the probability $p(R_k)$ satisfies the following normalizing condition

$$\int p(R_k)\, \mathrm{d}R_k = 1. \tag{3}$$

The expression of $\langle \Delta E_k \rangle$ defined in Eq. (2) is mathematically identical to the Gibbs entropy in statistical thermodynamics (Gibbs 1902). The variants of the Gibbs entropy, such as the Shannon entropy and Shannon–Wiener index, have been suggested in

a variety of subjects to quantify the heterogeneity of possible outcomes of a variable. For example, the Shannon entropy in information theory (Shannon 1948; Lin 1991) evaluates the mean level of information/uncertainty contained in a quantity, and the Shannon–Wiener index in ecology (Pielou 1966; Ludwig and Reynolds 1988) describes the spatial diversity of species in natural ecosystems. In this study, $\langle \Delta E_k \rangle$ in Eq. (2) measures the temporal heterogeneity of variation rates of the environmental variables characterizing the evolutionary processes of the Phanerozoic geological system.

The Earth system is regulated by a variety of intertwined geological and biological processes and feedback mechanisms, which not only shape the geological and geochemical environments but also help maintain Earth's habitability over geologic timescales (Lovelock 2016; Lenton 1998; Lenton and Watson 2013). The structures of natural complex systems, such as the planetary-scale geological system, are usually neither perfectly ordered nor perfectly disordered; instead, they lie at some intermediate levels between these two (Bak 2013; Anderson 1972; Prigogine 1980). The order of magnitude of environmental metrics may better describe the geological system's complexity and variability than precise values. In light of the steady-state evolution proposed by the Gaia hypothesis (Lovelock 2016; Lenton 1998; Lenton and Watson 2013), I assume that the average variation rate of environmental variables is maintained at a certain order of magnitude and obtain

$$\int p(R_k) \cdot \mathcal{O}(R_k)\, \mathrm{d}R_k \simeq \zeta, \tag{4}$$

where $\mathcal{O}(R_k) \sim \log R_k$ is the order of magnitude of R_k, and ζ is a constant.

While the interactions between life and the environment stabilize the Earth system (Lovelock 2016; Lenton 1998; Lenton and Watson 2013), the dissipative nature of individual physical and biological processes tends to drive the Earth system and its components away from steady states (Vallino and Algar 2016; Kleidon 2010). The maximum entropy production principle suggests that a nonlinear system with a high degree of freedom, such as the Earth system, tends to select the state that maximizes the change in entropy (under some external constraints) along its evolutionary trajectory (Dewar 2005; Kleidon and Lorenz 2004; Martyushev 2010). According to this principle, I calculate the maximum of the average change in entropy, $\langle \Delta E_k \rangle$ in Eq. (2), under the constraints of Eqs. (3) and (4). To do so, I write the following Lagrangian (Jaynes 1957)

$$\begin{aligned} \mathcal{L} = &- \int p(R_k) \cdot \log p(R_k)\, \mathrm{d}R_k + \theta \left(1 - \int p(R_k)\, \mathrm{d}R_k\right) \\ &+ \phi \left(\zeta - \int p(R_k) \cdot \log R_k\, \mathrm{d}R_k\right), \end{aligned} \tag{5}$$

where $\theta \in \mathbb{R}^+$ and $\phi \in \mathbb{R}^+$ are Lagrangian multipliers. I take the derivative of both sides in Eq. (5) with respect to $p(R_k)$ and get

$$\frac{\partial \mathcal{L}}{\partial p(R_k)} = -(\log p(R_k) + 1) - \theta - \phi \log R_k. \tag{6}$$

To obtain the maximum of the average change in entropy, I set $\partial \mathcal{L}/\partial p(R_k) = 0$, which gives

$$p(R_k) = R_k^{-\phi} \cdot \exp[-(\theta + 1)]. \tag{7}$$

When we conduct M measurements, the number of times that variation rates with the value R_k occur can be expressed as $N(R_k) = M \cdot p(R_k)$. I substitute Eq. (7) into this relation and obtain

$$N(R_k) \sim R_k^{-\phi}, \tag{8}$$

which is a general form of the scale-independent patterns presented in this study.

3.3 Implications

Studies of scale-independent behaviors generally focus on physical and biological systems on the modern Earth; less attention, however, has been paid to the paleoenvironment. The most well-known scale-independent pattern on the ancient Earth appeared in the Phanerozoic biological system—that is, the power law between the frequency and size of extinction events (Raup 1986; Bak 2013). This work shows for the first time that scale-independent patterns existed in the deep-time geological system as well. The systematic power-law patterns in the variation rates of three key variables characterizing Earth's surface environment—the atmospheric CO_2 level, global average temperature, and sea level—suggest that certain fundamental mechanisms should have been responsible for such patterns. Although scale-independent behaviors are commonly taken as hints at fundamental mechanisms behind the observed data, the specific mechanisms of many such patterns are not well understood (Bak 2013; Schroeder 2009). From the perspective of thermodynamics, I develop a simple model to derive a general form of the scale-independent variation rates presented in this study based on some physical principles and geosystem-specific assumptions. This minimalistic model is detached from the details of the complex geosystem and provides a conceptual interpretation for the power laws appearing in the environmental metrics. Nevertheless, this model does not explain why the power-law exponents take those specific values and what the physical/biological factors influencing these values are.

A variety of theories have been proposed to explain scale-independent patterns in nature. Some theories focus on specific physical or biological systems, while others attempt to offer universal interpretations for scale-independent behaviors. For example, to explain the well-known power laws between the frequency and size of extinction events in the Phanerozoic biological system (Raup 1986; Bak 2013), several specific models have been suggested in previous studies, such as the NK model of Kauffman and Johnsen (1991), the percolation model of Plotnick and McKinney (1993), and the random stress model of Newman (1997). Some of these models (e.g., the NK

and percolation models) have been ruled out while others (e.g., the random stress model) require further validation. On the other hand, with more fundamental physical principles, Bak et al. (1987) suggested self-organized criticality while Carlson and Doyle (1999) proposed the "highly optimized tolerance" mechanism to explain the universal mechanisms responsible for power laws. Although these theories offer plausible interpretations for scale-independent behaviors in a variety of natural systems (Bak et al. 1987; Carlson and Doyle 1999), scale-independent patterns do not necessarily derive from these mechanisms (Hergarten 2002; Solow 2005). Whether the self-organized criticality or "highly optimized tolerance" mechanism could explain the scale-independent variation rates of the Phanerozoic CO_2 level, global average temperature, and sea level (Fig. 1 and Table 1) requires future investigation.

The results in this work bring up a caution as well. In geological and geochemical studies, extraordinarily large values are generally viewed as anomalies and attributed to abnormal environments in certain periods. Some large events, such as the massive CO_2 emission in the Permian–Triassic transition and the Paleocene–Eocene Thermal Maximum event (McInerney and Wing 2011), have attracted much attention. However, other significant events may remain obscure since the seemingly anomalous data that actually manifest these events might have been discarded as outliers. Although excluding extreme data appears reasonable because doing so could generate normal distributions and preserve equilibrium explanations, discarding large values may also conceal power-law patterns and "throw the baby out with the bathwater" (Bak 2013). Thus, it is advisable to perform careful assessments prior to removing extreme data in geological/geochemical measurements.

The fundamental principles governing the geological and biological systems in the modern environments should be the same as or similar to those under the ancient conditions; the scale-independent patterns exhibited by the atmospheric CO_2 level, global average temperature, and sea level on the ancient Earth therefore have significant implications for the modern Earth's sustainability and habitability. From the perspective of statistical mechanics, these scale-independent patterns are likely to derive from the internal dynamics and interactions of various components of the planetary-scale geological and biological systems (Bak 2013; Schroeder 2009). Studies of global environmental change conventionally regard external factors (e.g., human activity) as major drivers of climate crises. Although external factors indeed influence the stability of Earth's surface environment, they primarily contribute to regulating the degree of freedom of the Earth system rather than instigating significant changes (Ehlers and Krafft 2006; Jacobson et al. 2000). The global biogeosystem, which is governed by complex and coupled feedback mechanisms, is usually resilient to the perturbations of external forces and able to maintain itself at steady states in many cases (Folke et al. 2010; Steffen et al. 2018). Moreover, the scale-independent variation rates presented in this study also suggest that the complex interactions of the components in the biogeosystem may be able to self-organize it into critical states where catastrophic events can occur. After all, extreme events in the Earth system can originate from internal interactions and do not require external forces as drivers. For instance, the interlocked feedback mechanisms in the deep-time biogeosystem might have resulted in the rapid accumulation of molecular oxygen on Earth's surface (Alcott et al. 2019; Laakso and Schrag 2017; Shang 2023c), abrupt changes in sedimentary records such as dolomite

and iron formations (Shang 2023a; Konhauser et al. 2017), and mass extinctions of life (Jablonski 2001; Bond and Grasby 2017; Bambach 2006) during short time periods. Therefore, the research on the modern Earth's sustainability and habitability should pay more attention to the intrinsic dynamics of the biogeosystem rather than focusing only on impacts induced by humans.

The significant role that internal dynamics and interactions play in Earth's stability also sheds light on climate change mitigation (Abbass et al. 2022) and ecosystem-based adaptation (Scarano 2017). With the advent of the Anthropocene, especially of the Industrial Revolution, gigantic amounts of CO_2 emission due to the utilization of coal, oil, and natural gas (Burnham et al. 2012; Yoro and Daramola 2020; Friedlingstein et al. 2010) have dramatically altered Earth's carbon cycle and other biogeochemical cycles tightly coupled with it and remarkably affected Earth's surface environments (e.g., increases in global average temperature and sea level) (Raupach and Canadell 2010; He and Silliman 2019; Summerhayes and Zalasiewicz 2018). While reducing the influence of human activity (e.g. CO_2 emission) is widely considered an effective way of mitigating climate change, taking advantage of the internal interactions in the biogeosystem provides an alternative solution for maintaining Earth's sustainability and habitability. New concepts and strategies for climate change mitigation and ecosystem-based adaptation such as blue carbon (Macreadie et al. 2021) and ocean nourishment (Iversen 2023), which take the latter approach, are expected to prevent the Earth system from heading toward more crises.

The evolutionary histories of geological and biological systems are correlated, suggesting that the scale-independent behaviors may also exist in the variation rates of metrics characterizing the deep-time biological system. Moreover, the fundamental physics governing the Phanerozoic geological system should have been the same during the Precambrian and potentially hold on Earth-like exoplanets. Such temporal and spatial universalities imply that the observational data of the geological quantities characterizing environmental changes, such as the evolution of biogeochemical cycles, on the Precambrian Earth and Earth-like exoplanets may exhibit scale-independent behaviors as well. These patterns may be viewed as snapshots of planetary-scale dynamical systems over geologic timescales.

Acknowledgements I thank Editor Roussos Dimitrakopoulos for handling this manuscript and two anonymous reviewers for thoughtful and constructive comments.

Author Contributions HS conceived the project, performed the research, and wrote the manuscript.

Declarations

Conflict of interest The author declares no conflict of interest.

References

Abbass K, Qasim MZ, Song H, Murshed M, Mahmood H, Younis I (2022) A review of the global climate change impacts, adaptation, and sustainable mitigation measures. Environ Sci Pollut Res 29(28):42539–42559. https://doi.org/10.1007/s11356-022-19718-6

Alcott LJ, Mills BJW, Poulton SW (2019) Stepwise Earth oxygenation is an inherent property of global biogeochemical cycling. Science 366(6471):1333–1337. https://doi.org/10.1126/science.aax6459
Almeida MP (2003) Thermodynamical entropy (and its additivity) within generalized thermodynamics. Physica A Stat Mech Appl 325(3–4):426–438. https://doi.org/10.1016/S0378-4371(03)00262-0
Alstott J, Bullmore E, Plenz D (2014) Powerlaw: a Python package for analysis of heavy-tailed distributions. PLoS ONE 9(1):e85777. https://doi.org/10.1371/journal.pone.0085777
Anderson TW (1962) On the distribution of the two-sample Cramér–von Mises criterion. Ann Math Stat 33:1148–1159. https://doi.org/10.1214/aoms/1177704477
Anderson PW (1972) More is different: broken symmetry and the nature of the hierarchical structure of science. Science 177(4047):393–396. https://doi.org/10.1126/science.177.4047.393
Bak P (2013) How nature works: the science of self-organized criticality. Springer, Berlin. https://doi.org/10.1007/978-1-4757-5426-1
Bak P, Tang C, Wiesenfeld K (1987) Self-organized criticality: an explanation of the 1/f noise. Phys Rev Lett 59(4):381. https://doi.org/10.1103/PhysRevLett.59.381
Bak P, Christensen K, Danon L, Scanlon T (2002) Unified scaling law for earthquakes. Phys Rev Lett 88(17):178501. https://doi.org/10.1073/pnas.012581099
Bambach RK (2006) Phanerozoic biodiversity mass extinctions. Annu Rev Earth Planet Sci 34:127–155. https://doi.org/10.1146/annurev.earth.33.092203.122654
Berner RA (1990) Atmospheric carbon dioxide levels over Phanerozoic time. Science 249(4975):1382–1386. https://doi.org/10.1126/science.249.4975.138
Bond DPG, Grasby SE (2017) On the causes of mass extinctions. Palaeogeogr Palaeoclimatol Palaeoecol 478:3–29. https://doi.org/10.1016/j.palaeo.2016.11.005
Boulila S, Laskar J, Haq BU, Galbrun B, Hara N (2018) Long-term cyclicities in Phanerozoic sea-level sedimentary record and their potential drivers. Glob Planet Change 165:128–136. https://doi.org/10.1016/j.gloplacha.2018.03.004
Burnham A, Han J, Clark CE, Wang M, Dunn JB, Palou-Rivera I (2012) Life-cycle greenhouse gas emissions of shale gas, natural gas, coal, and petroleum. Environ Sci Technol 46(2):619–627. https://doi.org/10.1021/es201942m
Cannavò F, Nunnari G (2016) On a possible unified scaling law for volcanic eruption durations. Sci Rep 6(1):22289. https://doi.org/10.1038/srep22289
Carlson JM, Doyle J (1999) Highly optimized tolerance: a mechanism for power laws in designed systems. Phys Rev E 60(2):1412. https://doi.org/10.1103/PhysRevE.60.1412
Clauset A, Shalizi CR, Newman MEJ (2009) Power-law distributions in empirical data. SIAM Rev 51(4):661–703. https://doi.org/10.1137/070710111
De Boor C (1978) A practical guide to splines, vol 27. Springer, New York
Dewar RC (2005) Maximum entropy production and the fluctuation theorem. J Phys A Math Gen 38(21):L371. https://doi.org/10.1088/0305-4470/38/21/L01
Ehlers E, Krafft T (2006) Earth system science in the Anthropocene. Springer, Berlin. https://doi.org/10.1007/b137853
Folke C, Carpenter SR, Walker B, Scheffer M, Chapin T, Rockström J (2010) Resilience thinking: integrating resilience, adaptability and transformability. Ecol Soc 15(4):9. https://doi.org/10.5751/es-03610-150420
Foster GL, Rohling EJ (2013) Relationship between sea level and climate forcing by CO_2 on geological timescales. Proc Natl Acad Sci 110(4):1209–1214. https://doi.org/10.1073/pnas.1216073110
Foster GL, Royer DL, Lunt DJ (2017) Future climate forcing potentially without precedent in the last 420 million years. Nat Commun 8(1):1–8. https://doi.org/10.1038/ncomms14845
Freund RJ, Wilson WJ (2003) Statistical methods. Elsevier, Amsterdam. https://doi.org/10.1016/C2019-0-02521-6
Friedlingstein P, Houghton RA, Marland G, Hackler J, Boden TA, Conway TJ, Canadell JG, Raupach MR, Ciais P, Le Quéré C (2010) Update on CO_2 emissions. Nat Geosci 3(12):811–812. https://doi.org/10.1038/ngeo1022
Gibbs JW (1902) Elementary principles in statistical mechanics: developed with especial reference to the rational foundations of thermodynamics. Cambridge University Press, Cambridge. https://doi.org/10.1017/CBO9780511686948
Hallam A, Wignall PB (1999) Mass extinctions and sea-level changes. Earth Sci Rev 48(4):217–250. https://doi.org/10.1016/S0012-8252(99)00055-0

Hannisdal B, Peters SE (2011) Phanerozoic Earth system evolution and marine biodiversity. Science 334(6059):1121–1124. https://doi.org/10.1126/science.1210695
Hayes JM, Waldbauer JR (2006) The carbon cycle and associated redox processes through time. Philos Trans R Soc B Biol Sci 361(1470):931–950. https://doi.org/10.1098/rstb.2006.1840
He Q, Silliman BR (2019) Climate change, human impacts, and coastal ecosystems in the Anthropocene. Curr Biol 29(19):R1021–R1035. https://doi.org/10.1016/j.cub.2019.08.042
Hergarten S (2002) Self organized criticality in Earth systems, vol 2. Springer, Heidelberg. https://doi.org/10.1007/978-3-662-04390-5
Huang Y, Schmitt FG (2014) Time dependent intrinsic correlation analysis of temperature and dissolved oxygen time series using empirical mode decomposition. J Mar Syst 130:90–100. https://doi.org/10.1016/j.jmarsys.2013.06.007
Iversen MH (2023) Carbon export in the ocean: a biologist's perspective. Annu Rev Mar Sci 15:357–381. https://doi.org/10.1146/annurev-marine-032122-035153
Jablonski D (2001) Lessons from the past: evolutionary impacts of mass extinctions. Proc Natl Acad Sci 98(10):5393–5398. https://doi.org/10.1073/pnas.101092598
Jacobson M, Charlson RJ, Rodhe H, Orians GH (2000) Earth system science: from biogeochemical cycles to global changes. Academic Press, Cambridge. https://doi.org/10.1016/s0074-6142(00)x8104-1
Jaynes ET (1957) Information theory and statistical mechanics. Phys Rev 106(4):620. https://doi.org/10.1103/PhysRev.106.620
Kauffman SA, Johnsen S (1991) Coevolution to the edge of chaos: coupled fitness landscapes, poised states, and coevolutionary avalanches. J Theor Biol 149(4):467–505. https://doi.org/10.1016/S0022-5193(05)80094-3
Kleidon A (2010) A basic introduction to the thermodynamics of the Earth system far from equilibrium and maximum entropy production. Philos Trans R Soc B Biol Sci 365(1545):1303–1315. https://doi.org/10.1098/rstb.2009.0310
Kleidon A, Lorenz RD (2004) Non-equilibrium thermodynamics and the production of entropy: life, Earth, and beyond. Springer, Heidelberg. https://doi.org/10.1007/b12042
Kocsis ÁT, Scotese CR (2021) Mapping paleocoastlines and continental flooding during the Phanerozoic. Earth Sci Rev 213:103463. https://doi.org/10.1016/j.earscirev.2020.103463
Konhauser KO, Planavsky NJ, Hardisty DS, Robbins LJ, Warchola TJ, Haugaard R, Lalonde SV, Partin CA, Oonk PBH, Tsikos H, Lyons TW, Bekkee A, Johnson CM (2017) Iron formations: a global record of Neoarchaean to Palaeoproterozoic environmental history. Earth Sci Rev 172:140–177
Laakso TA, Schrag DP (2017) A theory of atmospheric oxygen. Geobiology 15(3):366–384. https://doi.org/10.1111/gbi.12230
Lenton TM (1998) Gaia and natural selection. Nature 394(6692):439–447. https://doi.org/10.1038/28792
Lenton T, Watson A (2013) Revolutions that made the Earth. Oxford University Press, Oxford
Lin J (1991) Divergence measures based on the Shannon entropy. IEEE Trans Inf Theory 37(1):145–151. https://doi.org/10.1109/18.61115
Lovelock J (2016) Gaia: a new look at life on Earth. Oxford University Press, Oxford
Ludwig JA, Reynolds JF (1988) Statistical ecology: a primer in methods and computing, vol 1. Wiley, Hoboken
Macreadie PI, Costa MDP, Atwood TB, Friess DA, Kelleway JJ, Kennedy H, Lovelock CE, Serrano O, Duarte CM (2021) Blue carbon as a natural climate solution. Nat Rev Earth Environ 2(12):826–839. https://doi.org/10.1038/s43017-021-00224-1
Martyushev LM (2010) The maximum entropy production principle: two basic questions. Philos Trans R Soc B Biol Sci 365(1545):1333–1334. https://doi.org/10.1098/rstb.2009.0295
Massey FJ Jr (1951) The Kolmogorov–Smirnov test for goodness of fit. J Am Stat Assoc 46(253):68–78. https://doi.org/10.1080/01621459.1951.10500769
Mayhew PJ, Bell MA, Benton TG, McGowan AJ (2012) Biodiversity tracks temperature over time. Proc Natl Acad Sci 109(38):15141–15145. https://doi.org/10.1073/pnas.120084410
McInerney FA, Wing SL (2011) The paleocene–eocene thermal maximum: a perturbation of carbon cycle, climate, and biosphere with implications for the future. Annu Rev Earth Planet Sci 39:489–516. https://doi.org/10.1146/annurev-earth-040610-133431
Middelburg JJ (1989) A simple rate model for organic matter decomposition in marine sediments. Geochim Cosmochim Acta 53(7):1577–1581. https://doi.org/10.1016/0016-7037(89)90239-1
Newman MEJ (1997) A model of mass extinction. J Theor Biol 189(3):235–252. https://doi.org/10.1006/jtbi.1997.0508

Peters SE (2005) Geologic constraints on the macroevolutionary history of marine animals. Proc Natl Acad Sci 102(35):12326–12331. https://doi.org/10.1073/pnas.0502616102
Peters SE (2007) The problem with the Paleozoic. Paleobiology 33(2):165–181. https://doi.org/10.1666/06067.1
Pielou EC (1966) Shannon's formula as a measure of specific diversity: its use and misuse. Am Nat 100(914):463–465. https://doi.org/10.1086/282439
Plotnick RE, McKinney ML (1993) Ecosystem organization and extinction dynamics. Palaios 8:202–212. https://doi.org/10.2307/3515172
Prigogine I (1980) From being to becoming: time and complexity in the physical sciences. Freeman, New York
Raup DM (1986) Biological extinction in Earth history. Science 231(4745):1528–1533. https://doi.org/10.1126/science.11542058
Raupach MR, Canadell JG (2010) Carbon and the Anthropocene. Curr Opin Environ Sustain 2(4):210–218. https://doi.org/10.1073/pnas.0907765106
Royer DL, Berner RA, Beerling DJ (2001) Phanerozoic atmospheric CO_2 change: evaluating geochemical and paleobiological approaches. Earth Sci Rev 54(4):349–392. https://doi.org/10.1016/S0012-8252(00)00042-8
Scarano FR (2017) Ecosystem-based adaptation to climate change: concept, scalability and a role for conservation science. Perspect Ecol Conserv 15(2):65–73. https://doi.org/10.1016/j.pecon.2017.05.003
Schroeder M (2009) Fractals, chaos, power laws: minutes from an infinite paradise. Courier Corporation, Massachusetts
Scotese CR, Song H, Mills BJW, van der Meer DG (2021) Phanerozoic paleotemperatures: the Earth's changing climate during the last 540 million years. Earth Sci Rev 215:103503. https://doi.org/10.1016/j.earscirev.2021.103503
Scott DW (2009) Sturges' rule. Wiley Interdiscip Rev Comput Stat 1(3):303–306. https://doi.org/10.1002/wics.35
Shang H (2023a) Dichotomous effects of oxidative metabolisms: a theoretical perspective on the dolomite problem. Glob Planet Change 222:104041. https://doi.org/10.1016/j.gloplacha.2023.104041
Shang H (2023b) A generic hierarchical model of organic matter degradation and preservation in aquatic systems. Commun Earth Environ 4:16. https://doi.org/10.1038/s43247-022-00667-4
Shang H (2023c) Mineral evolution facilitated Earth's oxidation. Commun Earth Environ 4:213. https://doi.org/10.1038/s43247-023-00824-3
Shannon CE (1948) A mathematical theory of communication. Bell Syst Tech J 27(3):379–423. https://doi.org/10.1002/j.1538-7305.1948.tb01338.x
Skilling J (1989) Classic maximum entropy. In: Skilling J (ed) Maximum entropy and Bayesian methods. Springer, Berlin, pp 45–52. https://doi.org/10.1007/978-94-017-2219-3
Solow AR (2005) Power laws without complexity. Ecol Lett 8(4):361–363. https://doi.org/10.1111/j.1461-0248.2005.00738.x
Song H, Wignall PB, Song H, Dai X, Chu D (2019) Seawater temperature and dissolved oxygen over the past 500 million years. J Earth Sci 30(2):236–243. https://doi.org/10.1007/s12583-018-1002-2
Song H, Kemp DB, Tian L, Chu D, Song H, Dai X (2021) Thresholds of temperature change for mass extinctions. Nat Commun 12(1):1–8. https://doi.org/10.1038/s41467-021-25019-2
Steffen W, Rockström J, Richardson K, Lenton TM, Folke C, Liverman D, Summerhayes CP, Barnosky AD, Cornell SE, Crucifix M, Donges JF (2018) Trajectories of the Earth system in the Anthropocene. Proc Natl Acad Sci 115(33):8252–8259. https://doi.org/10.1073/pnas.1810141115
Summerhayes CP, Zalasiewicz J (2018) Global warming and the Anthropocene. Geol Today 34(5):194–200. https://doi.org/10.1111/gto.12247
Vallino JJ, Algar CK (2016) The thermodynamics of marine biogeochemical cycles: Lotka revisited. Annu Rev Mar Sci 8:333–356. https://doi.org/10.1146/annurev-marine-010814-015843
Vérard C, Veizer J (2019) On plate tectonics and ocean temperatures. Geology 47(9):881–885. https://doi.org/10.1130/G46376.1
Vuong QH (1989) Likelihood ratio tests for model selection and non-nested hypotheses. Econom J Econom Soc 57:307–333. https://doi.org/10.2307/1912557
Yoro KO, Daramola MO (2020) CO_2 emission sources, greenhouse gases, and the global warming effect. In: Rahimpour MR, Farsi M, Makarem MA (eds) Advances in carbon capture. Elsevier, Amsterdam, pp 3–28. https://doi.org/10.1016/B978-0-12-819657-1.00001-3